Identifying at molecular scale the pyrolysis heavy components from two lignin monomers

Yi Qiu, Dian Zhong, Kuo Zeng, Jun Li, Gilles Flamant, Ange Nzihou, Haiping Yang, Hanping Chen

Identifying at molecular scale the pyrolysis heavy components from two lignin monomers

Yi Qiu [a], Dian Zhong [b], Kuo Zeng [a,b,*], Jun Li [b], Gilles Flamant [c], Ange Nzihou [d,e,f], Haiping Yang [b], Hanping Chen [b]

[a] China-EU Institute for Clean and Renewable Energy, Huazhong University of Science and Technology, Wuhan 430074, PR China
[b] State Key Laboratory of Coal Combustion, Huazhong University of Science and Technology, 1037 Luoyu Road, Wuhan, Hubei 430074, PR China
[c] Processes, Materials and Solar Energy Laboratory, PROMES-CNRS, 7 rue du Four Solaire, 66120 Odeillo Font Romeu, France
[d] Université de Toulouse, IMT Mines Albi, RAPSODEE CNRS UMR 5302, Campus Jarlard, F.81013 Albi Cedex 09, France
[e] Princeton University, School of Engineering and Applied Science, Princeton, NJ 08544, USA
[f] Princeton University, Andlinger Center for Energy and the Environment, Princeton, NJ 08544, USA

A B S T R A C T

4-hydroxy benzaldehyde (H) and vanillin (G) are typical primary pyrolysis products of β-O-4 lignin dimers with key functional groups that affect the secondary reactions of lignin pyrolysis. In this study, the pyrolysis heavy components from these two lignin monomers were analyzed and identified at molecular scale for the first time with Fourier transform-ion cyclotron resonance mass spectrometry (FT-ICR-MS) and compared with lignin-derived results. The detected heavy components were typically phenolic oligomers distributed in the nominal mass range of 200–600 Da with 2–6 aromatic rings. They are assumed to be formed through the re-polymerization of certain GC-MS-detected monomers during pyrolysis. In particular, the extra methoxy group in model compound G allows for more variations of monomer products, which serve as building blocks to form heavy components and char. Two-dimensional Kendrick mass defect (2D KMD) analysis was employed to reveal the evolution of different functional groups. Two evolution pathways were found to be dominant, namely the modification of phenol cores and methoxy groups. It was found that aldehyde groups promoted the evolution of heavy components with more aromatic rings (up to 6), which might serve as precursors for char. This influence was mitigated by the co-existence of methoxy group, which might compete for the linking positions on benzene rings.

1. Introduction

Replacing fossil fuels with more sustainable alternatives has remained one of the most serious challenges in the 21st century [1–3]. Lignin is an attractive candidate, which is widely available, carbon–neutral and nonedible [2,4]. The abundant content of aromatic building blocks makes lignin a suitable starting material to produce bio-based products as substitutes for currently used, petroleum-derived BTX (benzene, toluene, and xylene) [2,5,6]. However, lignin as well as other biomass materials is solid, highly oxygenated and extremely heterogeneous, which is very different from petroleum [7–9]. Naturally, lignin is formed by free radical polymerization of three main monolignols (Fig. 1) in the plant cell wall: p-coumaryl alcohol, coniferyl alcohol, and sinapyl alcohol [1,4]. These chemical components differ in the number of methoxy groups attached to the phenolic nucleus, commonly denoted as H (p-hydroxyphenyl), G (guaiacyl), and S (syringyl), respectively. Moreover, these monolignols are connected by various inter-unit linkages including both ether and carbon–carbon bonds [10,11], which makes lignin polymers highly complex heterogeneous materials. Therefore, the full characterization of the individual monolignols at molecular scale is required to assess the desired high value chemicals from these polymers [12].

Pyrolysis is a desirable thermochemical technology for the conversion of solid biomass into higher value carbonaceous solids and liquid hydrocarbons. During pyrolysis the ether and carbon–carbon linkages in lignin are broken down to form the primary products, mostly monolignols with various H or G units [13–16]. However, these primary products are usually highly reactive and tend to polymerize to more complex and undesirable heavy components [17]. In order to unlock the mechanism of lignin pyrolysis, abundant researches have been

* Corresponding author.

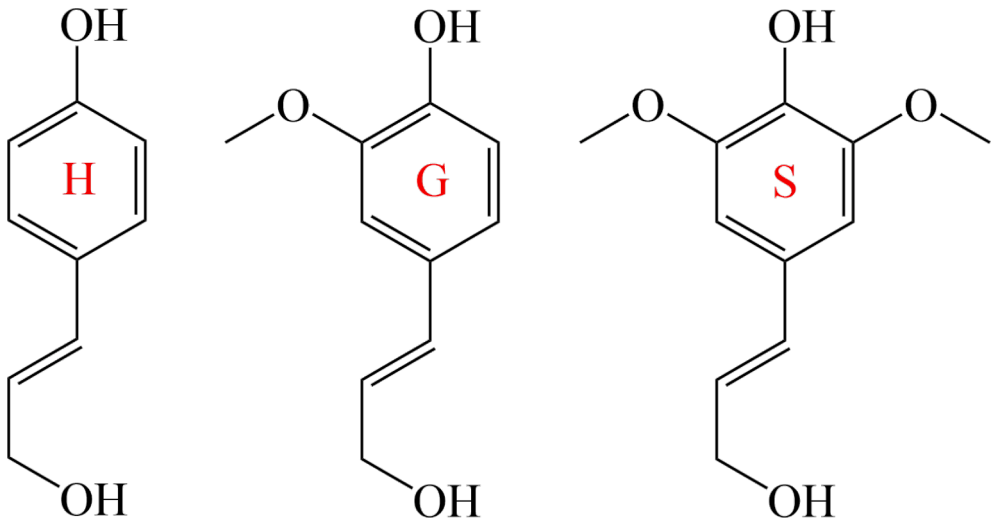

Fig. 1. Chemical structures of three main monolignols: p-coumaryl alcohol (H), coniferyl alcohol (G), and sinapyl alcohol (S).

conducted with model compounds that can represent the three monolignols as well as their various bonds. In the study of Asmadi et al. [18], two reaction pathways for lignin aromatic nuclei were revealed, namely the homolysis of the O-CH_3 bond to form methyl and pyrocatechol radicals and radical-induced rearrangement of aromatic OCH_3 into aromatic CH_3 structure. Jiang et al. [19] utilized vanillin and acetovanillone as two representative lignin monomers and found that the side-chain-conversion is more likely to occur on the aryl-CHO and aryl-OCH_3 groups rather than the aryl-$COCH_3$ groups. In these and other studies [18–21], the low molecular weight species (MW $<$ 400 Da) in the pyrolysis products were detected using one- or two-dimensional gas chromatography (GC or GC $\times$ GC), ultraviolet fluorescence (UV-F) spectroscopy, nuclear magnetic resonance (NMR), gel permeation chromatography (GPC) among other techniques [22,23]. These analyses allow for a comprehensive characterization of up to 20 % of the product mass extractable by organic solvents, while large fraction of lignin-oil, mostly heavy components with MW $>$ 200 Da, is not detectable by GC due to the high boiling point of the chemical species [22,24]. Thus, for mixtures as complex as lignin pyrolysis products, effective identification and analysis for the GC-undetectable heavy components are very necessary [25–27]. This will help to further establish lignin pyrolysis mechanisms at molecular scale and promote the entire biorefinery process [17].

Fourier transform-ion cyclotron resonance mass spectrometry (FT-ICR-MS) is a robust method with successful applications for detailed molecular analysis in related fields like petroleomics [28–30] and natural or dissolved organic matter [31–33]. Among many other mass spectrometry-based tools [23,27,34], FT-ICR-MS is particularly suitable for lignin characterization with its ultrahigh resolving power (>200,000) and wide detection range (MW of 200–1000 Da) [35,36]. Due to these advantages, the ion mass detected by the FT-ICR-MS can be used to calculate the accurate chemical formula of each heavy component [37–39]. Although the complexity of pyrolytic heavy components has been greatly reduced with the use of model compounds, there are still thousands of compounds detected in each experimental group. Therefore, visualization and structural interpretations of the spectra are important and require special technics [40], including Kendrick mass defect (KMD) analysis [41], the van Krevelen diagram [35,39] and double bond equivalence (DBE) vs carbon number distribution plots [42,43]. In our previous study, these visualization methods have been successfully employed to investigate the evolution of heavy components in bio-oil from the pyrolysis of cellulose, hemicellulose and lignin [38,44], as well as the evolution of nitrogen-containing heavy species in algae pyrolysis bio-oil [37]. In particular, the Kendrick mass defect (KMD) analysis enabled the alignment of thousands of mass peaks across the *m/z* range according to their homologous structural units [40,41], which would be prominent in the pyrolysis heavy oil from functional-group-controlled model compounds used in this study. The utilization of Kendrick mass defect (KMD) analysis has been expanded by Qi et al. [12], who has developed the so-called two-dimensional Kendrick mass defect (2D KMD) matrix plots, which greatly simplified the highly convoluted lignin mass spectral data and provided confident peak assignments and superior structural mapping of lignin decomposition product series.

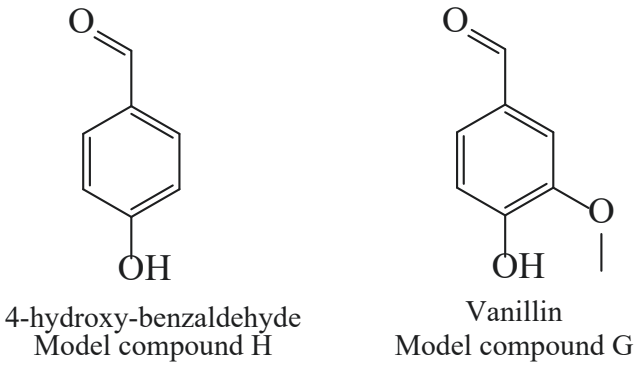

Fig. 2. Chemical structures of model compound H (left) and G (right).

In the present study, two lignin monomers, 4-hydroxy benzaldehyde (H) and vanillin (G) were chosen as model compounds (Fig. 2). Model compound H has an aldehyde group attached to its phenol core; while model compound G has an extra methoxy group. As suggested by Hosoya et al. [16], the methoxyl group was a key structure for lignin char formation, whose influence is also of interest to reveal the evolution mechanism of heavy components that are widely believed to be important char precursors. Model compounds H and G were pyrolyzed at 400, 500, 600 and 700 °C and the liquid products were analyzed with FT-ICR-MS for identification of pyrolytic heavy components. Two-dimensional Kendrick mass defect analysis (2D KMD) [12] was employed to reveal the evolution of different functional groups. With this approach, FT-ICR mass spectra can be simplified and visualized in a way that allows for (1) identifying possible reaction pathways, and (2) structural mapping of homogeneous series from the pyrolysis heavy components of lignin model compounds.

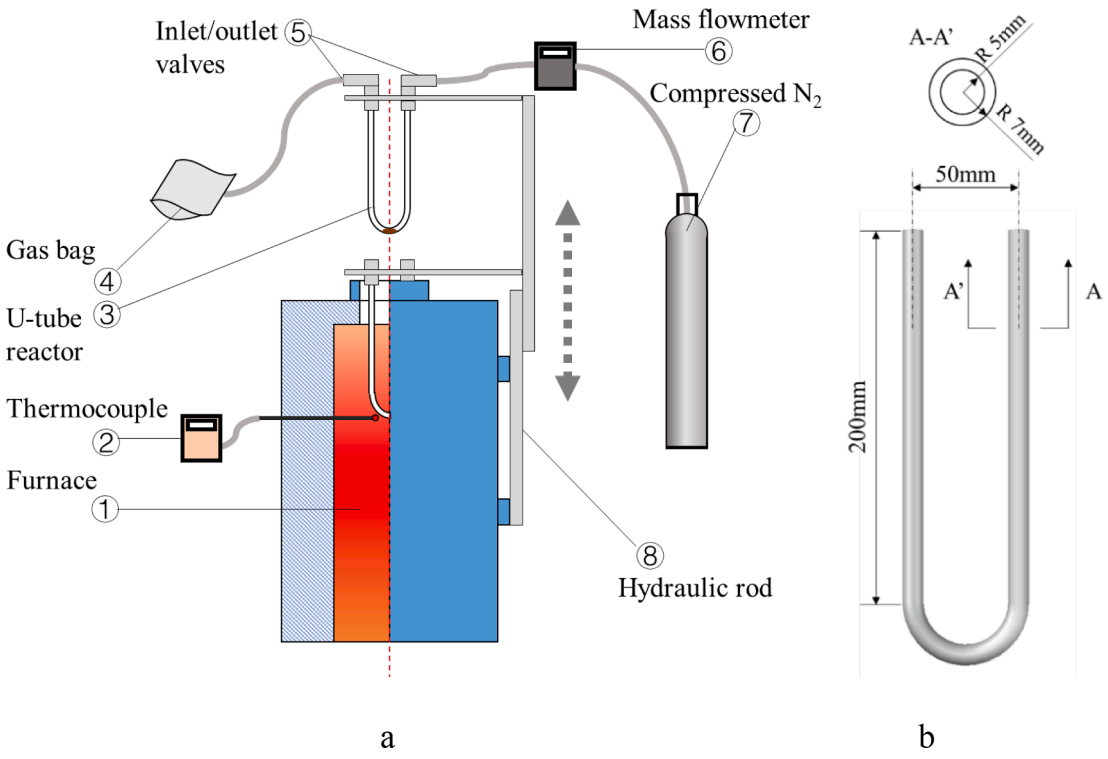

Fig. 3. The closed pyrolysis system (a) and the U-tube reactor (b) [38].

2. Materials and methods

2.1. Materials

Model compounds 4-hydroxybenzaldehyde (CAS 123-08-0), 4-hydroxy-3-methoxy-benzaldehyde (CAS 121-33-5) and alkali lignin (CAS 8068-05-1) were supplied by Sigma-Aldrich Pte. ltd. with purity higher than 98 %. The model compounds were used without further purification. Lignin samples have been dried at 105 °C for 4 h before use. The proximate and ultimate analyses of lignin sample can be found in our previous study [38].

2.2. Experiments

The experiment was conducted in a closed reaction device shown in Fig. 3a. The system includes a vertical tube furnace (OTF-1200X-4-VTQ) and a quartz U-tube reactor. The specific size of the reactor is shown in Fig. 3b.

Before pyrolysis, 100 mg sample was loaded in the U-tube reactor, and then the system was flushed by N_2 (99.999 %, 300 ml/min) for 3 min. The thermocouple was placed at a depth of 250 mm from the entrance of the furnace to measure the temperature of reaction zone. Once the target temperature was reached (400 °C, 500 °C, 600 °C, 700 °C), the gas inlet and outlet valves were closed immediately, and the reactor was quickly lowered down to the center of the furnace. Considering the small reactor size and sample amount, the heat transfer is assumed very quick compared to reaction time (240 s). After pyrolysis, the reactor was taken out immediately and cooled with compressed air for 2 min and subsequently immersed in ice-water mixture for 1 min. Then the valves were open again, allowing uncondensed gas to be wiped out by N_2 (99.999 %, 300 ml/min) for 3 min. The gas was collected by gas bag for further analysis. The liquid products condensed in the reactor was extracted with CH_3OH (LC/MS grade, purity ≥ 99.9 %) to form a 10 ml solution. The dark-colored residue that could not be dissolved, as well as the solid product, were together defined as char fraction in this paper.

Table 1
The rules applied for assignment of chemical formulas.

Items	Rules	Reference
C number	$^{12}C \leq 50$; $^{13}C \leq 2$	[52]
H number	$^{1}H \leq 100$; H/C ≤ 2.35	
O number	$^{16}O \leq 30$; O/C ≤ 2	
Relative error	≤ 3 ppm	[45]
Absolute error	$\leq 10^{-3}$	[37]
DBE (Double Bond Equivalent)	Positive integer	[53]
Others	*N*-rules	[51]

2.3. Product analysis

2.3.1. Gas product

The gas products were qualitatively and quantitatively analyzed using a dual-channel micro-gas chromatography (Panna A91 GC) equipped with a thermal conductivity detector (TCD) and a hydrogen flame ionization detector (FID).

2.3.2. FT-ICR-MS analysis

FT-ICR-MS (Bruker, Solarix 7.0 T) was used to analyze the heavy compounds in bio-oil in negative mode using electrospray ionization (ESI) source, which has been reported effective for polar compounds (N, O, and S heteroatoms) in MS analysis [45,46]. Furthermore, the negative ion mode (ESI(-)) was chosen instead of the positive one (ESI(+)) because the raw materials do not contain nitrogen or sulfur, which are preferred by ESI(+) [37]. Before analysis, the bio-oil was diluted with CH_3OH (LC/MS grade) to 0.4 mg/ml for a better ionization and separation in the FT-ICR-MS [47–49], and the instrument was calibrated by NaCOOH (≥99.99 %) solution [50]. Then the sample was infused into the MS at a rate of 120 μml/h. Each spectrum was gained after co-adding 128 scans to enhance the signal-to-noise ratio (S/N). After acquisition, the mass spectra data were loaded into Bruker DataAnalysis 4.2 software for calibration. The full scan mass spectra were internally calibrated using a series of homologous compounds throughout the detected *m/z* range. Elemental formulas were assigned to the peaks inside the

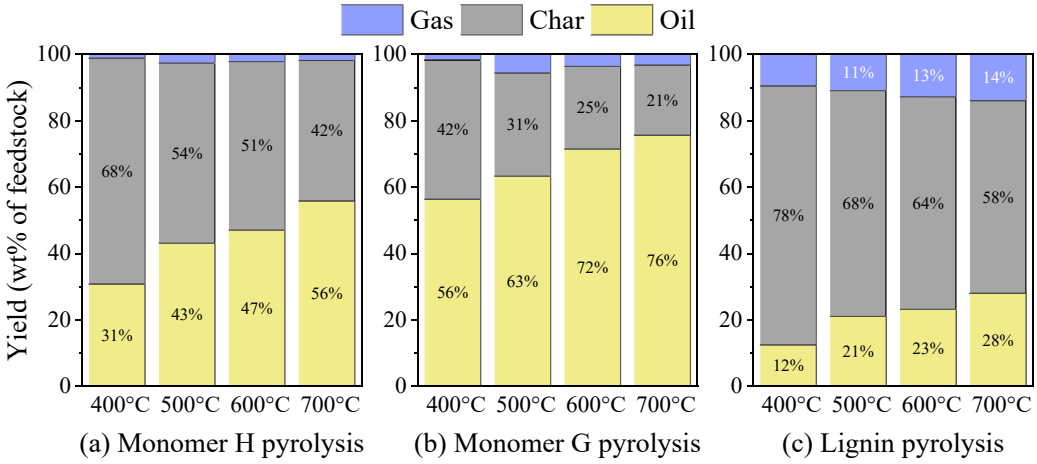

Fig. 4. Yields of bio-oil, char and gas from pyrolysis of model compounds H, G and alkali lignin.

calibrated *m/z* range. The signals with signal to noise ratio (S/N) ≥ 3 [51] were selected for further assignment using MATLAB script with tolerances listed in Table 1 to filter the formulas [37,38]. Besides, the solvent used to dilute the oil sample was also analyzed, and the prominent signals in solvent mass spectrum were abandoned in the experiment results.

2.3.3. KMD analysis

Each peak with an exact chemical formula assignment ($C_xH_yO_Z$) from FT-ICR-MS has a relative molecular mass (RM), which takes ^{12}C (12.000000 Da) as the mass reference. The original KMD plot [41] takes CH_2 unit as mass reference to derive Kendrick mass:

$$KM(CH_2) = RM \times \frac{14.00000}{14.01565}$$

It follows that compounds differing in chemical formulas with integer number of CH_2 units will have identical Kendrick mass defects (KMD):

$$KMD(CH_2) = KM(CH_2) - RM$$

This approach can be extended to other functional groups of interest by replacing CH_2 with any functional group F:

$$KM(F) = RM \times \frac{NM_F}{RM_F} \quad (3)$$

$$KMD(F) = KM(F) - RM \quad (4)$$

where RM_F is the relative molecular weight of group F, and NM_F is the nominal molecular weight of group F, which is relative molecular weight after rounding.

3. Results and discussion

3.1. Product distribution

Fig. 4 exhibits the pyrolysis products distribution of model compounds H, G and lignin [38]. Obvious differences can be spotted between lignin and its model compounds, as lignin generates much more char fraction and very little oil fraction [54]. Compared with model compounds, lignin has more abundant side chain structures and oxygen containing functional groups, which were suggested as key structures for char formation [16]. Existence of carbonyl groups in model compound H favors the formation of char [55], and this influence might be mitigated by the existence of methoxy groups (in case of model compound G). The rising temperature shows similar influence on lignin and monomeric model compounds, which promotes oil yields and inhibits char formation. In all temperature groups, little gas fraction was found in model compounds and its composition is listed in Table 2. Carbon monoxide is the most dominant gas product in both monomer H and G pyrolysis, which is produced by the dissociation of –CHO and was confirmed as typical gas product of vanillin [13]. More CH_4 was generated in G pyrolysis than in H pyrolysis, which is formed though the O–CH_3 bond homolysis of the aromatic rings [54].

The monomeric aromatics of the oil fractions obtained from pyrolysis of model compound H and G were investigated by GC-MS with their distribution shown in Table 3. It should be noted that monomeric liquid products only account for a modest percentage of the total oil yields [19,22]. Nevertheless, their structures and relative content are useful information for deducing the evolution of heavy components (mostly

Table 2
Gas composition from pyrolysis of model compounds H and G.

Temperature	Gas composition (vol. %)					HHV(MJ/Nm^3)
Monomer H	H_2	CO_2	CO	CH_4	C_2-C_5	
400 °C	–	–	96.43	3.57	–	13.43
500 °C	–	–	99.25	0.56	0.19	12.83
600 °C	–	–	97.90	1.68	0.42	13.22
700 °C	37.03	–	55.35	7.62	–	13.70
Monomer G	H_2	CO_2	CO	CH_4	C_2-C_5	
400 °C	–	–	88.66	11.34	–	15.23
500 °C	–	–	79.82	19.78	0.40	17.41
600 °C	–	–	78.25	20.89	0.86	17.91
700 °C	–	–	76.31	22.46	1.23	18.47

- Not detected.

Table 3
Peak area percentage (%) of GC–MS-obtained compounds from pyrolysis of model compounds H and G.

Sample	RT./ min	Monomers	Pyrolysis temperature/ °C			
			400	500	600	700
H	10.818	Phenol	2.78	42.15	62.83	79.10
	15.174	4-Methyl-phenol	–	0.37	0.10	1.47
	22.455	4-Hydroxy benzaldehyde*	97.11	57.13	34.50	15.00
G	11.300	Phenol	–	1.64	11.05	12.33
	13.110	2-Methyl-phenol	–	9.65	38.44	43.54
	13.917	Guaiacol	14.93	15.61	1.17	2.95
	18.326	Catechol	–	2.26	11.87	5.71
	23.555	Vanillin*	82.08	55.48	4.29	7.02
	23.914	4-Hydroxy-3-methyl-benzaldehyde	–	6.20	5.25	4.99

*Original sample.

Table 4
Classification of H/G-produced pyrolytic oligomers with different NAU based on their DBE values.

H	NAU	1	2	3	4	5	6	Unspecified
	DBE	4–5	8–10	12–15	16–19	20–25	26–28	Others
G	NAU	1	2	3	4	–	–	Unspecified
	DBE	4–5	8–10	12–15	16–20	–	–	Others

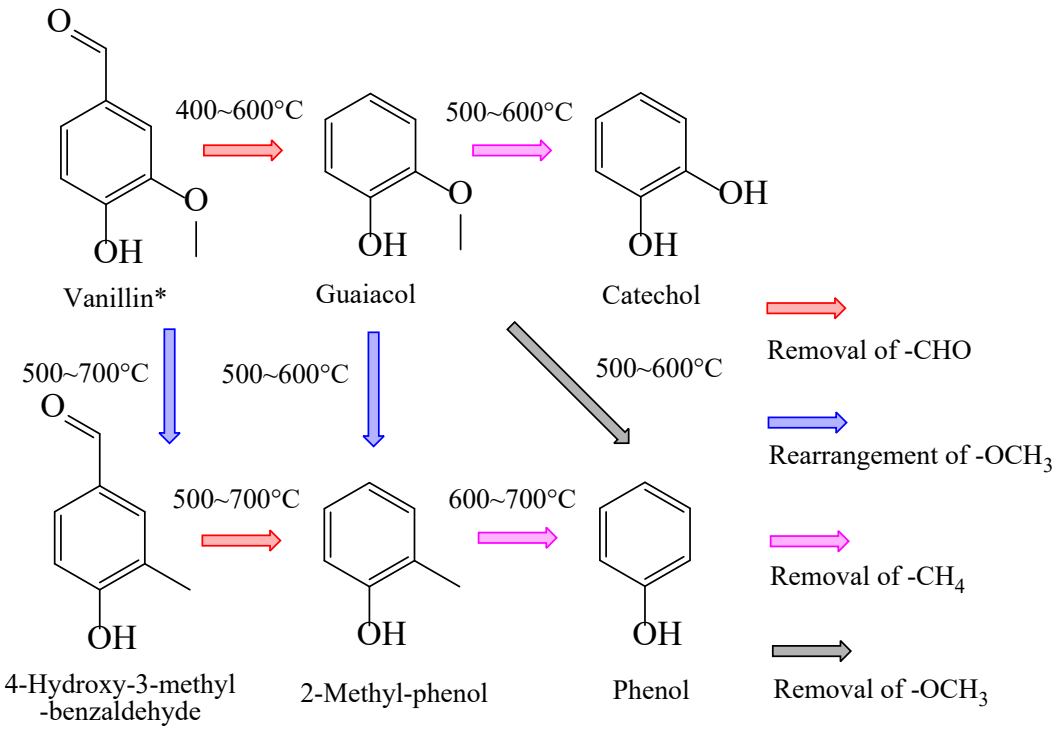

Fig. 5. Proposed reaction pathways of vanillin-derived monomers during pyrolysis.

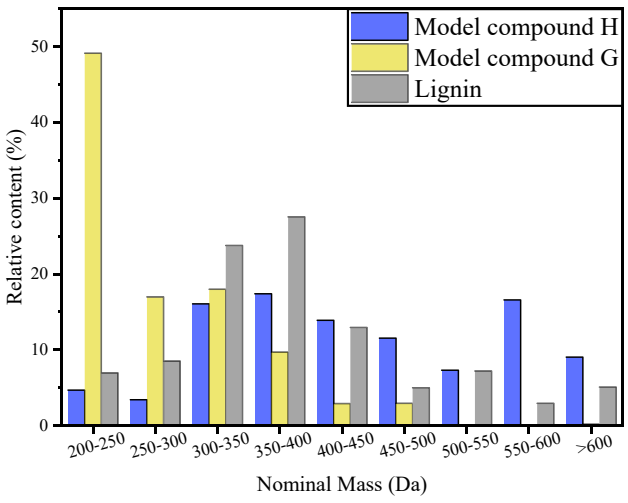

Fig. 6. Mass distribution of heavy components from pyrolysis of model compounds H, G and lignin (N_2/600 °C).

oligomers formed by the secondary reaction of these monomers) that are undetectable by GC-MS (Table 4).

Most of the model compounds H and G remain unreacted at 400 °C. From 400 °C to 500 °C, phenol and guaiacol were first generated through the removal of –CHO in the pyrolysis of H and G, respectively. From 500 °C to 700 °C, phenol continues to be generated in H-pyrolysis monomers, producing CO in the meantime (Table 2); while guaiacol is intensively transformed to phenol or 2-methyl-phenol through the removal of –OCH_3 group or the rearrangement of the aryl-OCH_3 group into the aryl-CH_3 group, respectively [19,56]. The later reaction pathway is also possible though not so intensive for the original monomer G, during which 4-hydroxy-3-methyl-benzaldehyde is generated and can be further transformed to 2-methyl-phenol. Removal of -CH_4 happens on the phenol cores of guaiacol and 2-methyl-phenol to form catechol and phenol, respectively [56]. The above proposed side-chain conversion pathways are summarized in Fig. 5. The extra methoxy group in model compound G allows for more variations of monomer products, which may serve as building blocks to form heavy components and char.

3.2. *General distribution and classification of heavy components*

The mass distribution of heavy components at 600 °C is presented with relative content calculated by the ratio of the summed abundance of detected components in the corresponding mass range to that of all heavy components under study (Fig. 6). Results of other temperature sets are presented in supplementary information (Fig. S1). The mass distribution of lignin-derived heavy components has obvious resemblances with that of H-derived heavy components, as both have a concentration in the mass range of 300–450 Da and a wide distribution over the mass range of 500–600 Da and above. Heavy components in the later mass range (>500 Da) are normally oligomers with>4 aromatic

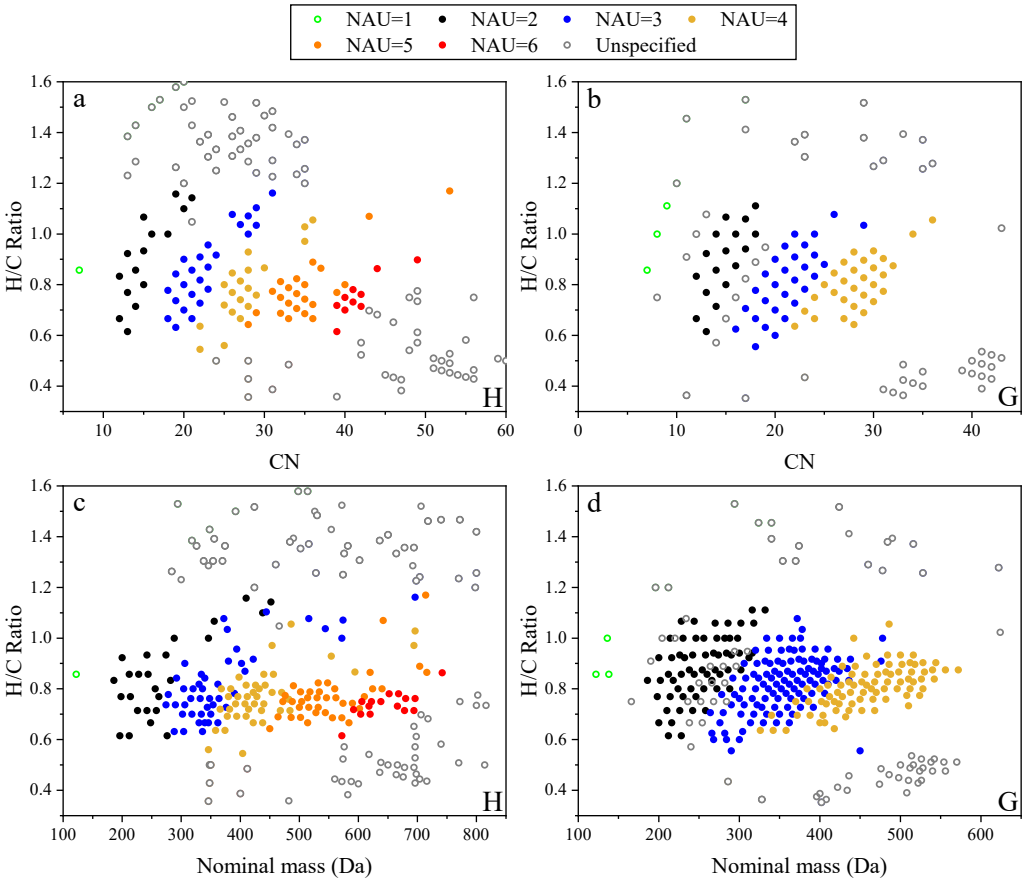

Fig. 7. Clusters of heavy components with different NAU presented on: a) H/C ratio vs CN plot for H-derived oligomers; b) H/C ratio vs CN plot for G-derived oligomers; c) H/C ratio vs nominal mass plot for H-derived oligomers; d) H/C ratio vs nominal mass plot for G-derived oligomers.

rings and might serve as precursors of char, which explains the higher char yields of model compound H than that of model compound G (Fig. 4). It is worth noting that as temperature rises from 400 °C to 600 °C, relative content of this mass range continues to shrink, consistent with the shrinking char fraction and enlarging oil fraction (Fig. 4). On the contrary, for G-derived components, relative content is the highest (49.1 %) in the mass range of 200–250 Da and continues to decline through 250–500 Da.

Double bond equivalent (DBE) is used to determine the number of aromatics (NAU) within the pyrolytic oligomers (Table 3). The classification standard for H/G-derived oligomers has been carefully checked considering all the possible combinations of their monomeric building blocks (Table 3). Based on the classification, clusters of oligomers with different NAU are presented in plots of H/C ratio vs nominal mass (NM) and H/C ratio vs carbon number (CN) (Fig. 7) [26]. With such visualization methods, it is possible to deduce the synchronous evolution of oligomers with growing automatic rings.

Different aromatic rings are readily distinguished by their H/C ratio and CN or nominal mass (Fig. 7). Model compound H tends to form oligomers with more aromatic rings (up to 6) through re-polymerization during pyrolysis, while model compound G only produces oligomers with up to 4 aromatic rings. Interestingly, fewer points are presented on H/C ratio vs CN plots (Fig. 7a, 4b) because some detected oligomers are overlapped with the same H/C ratio and carbon number. These overlapped oligomers could have different oxygen number and may evolve thorough the modification of hydroxyl groups. The unspecified heavy components are distributed into two relatively separate regions, with H/C ratio either higher than 1.2 or lower than 0.5. The former components (H/C $>$ 1.2) could be some unsaturated hydrocarbons or lipids, produced by benzene ring opening reactions or recombination of small radicals, both of which are typical reaction pathways during lignin pyrolysis [38]. The later components (H/C $<$ 0.5) are likely to be formed

Table 5
Average characteristics of the segregated clusters in Fig. 6.

NAU	Carbon number		Nominal mass		H/C ratio		DBE	
	H	G	H	G	H	G	H	G
1	7.000	7.800	122.000	139.600	0.857	0.965	5.000	5.000
2	14.600	14.738	269.840	252.689	0.850	0.882	9.240	9.164
3	21.826	21.450	369.217	355.413	0.819	0.820	13.696	13.587
4	27.238	28.120	438.476	457.325	0.773	0.802	17.571	17.759
5	34.800	–	554.500	–	0.775	–	22.150	–
6	41.353	–	662.824	–	0.748	–	26.824	–
Unspecified	31.466	24.161	564.733	388.151	1.211	1.090	16.389	13.903
Total	28.930	22.385	495.682	367.259	0.976	0.900	16.864	13.766

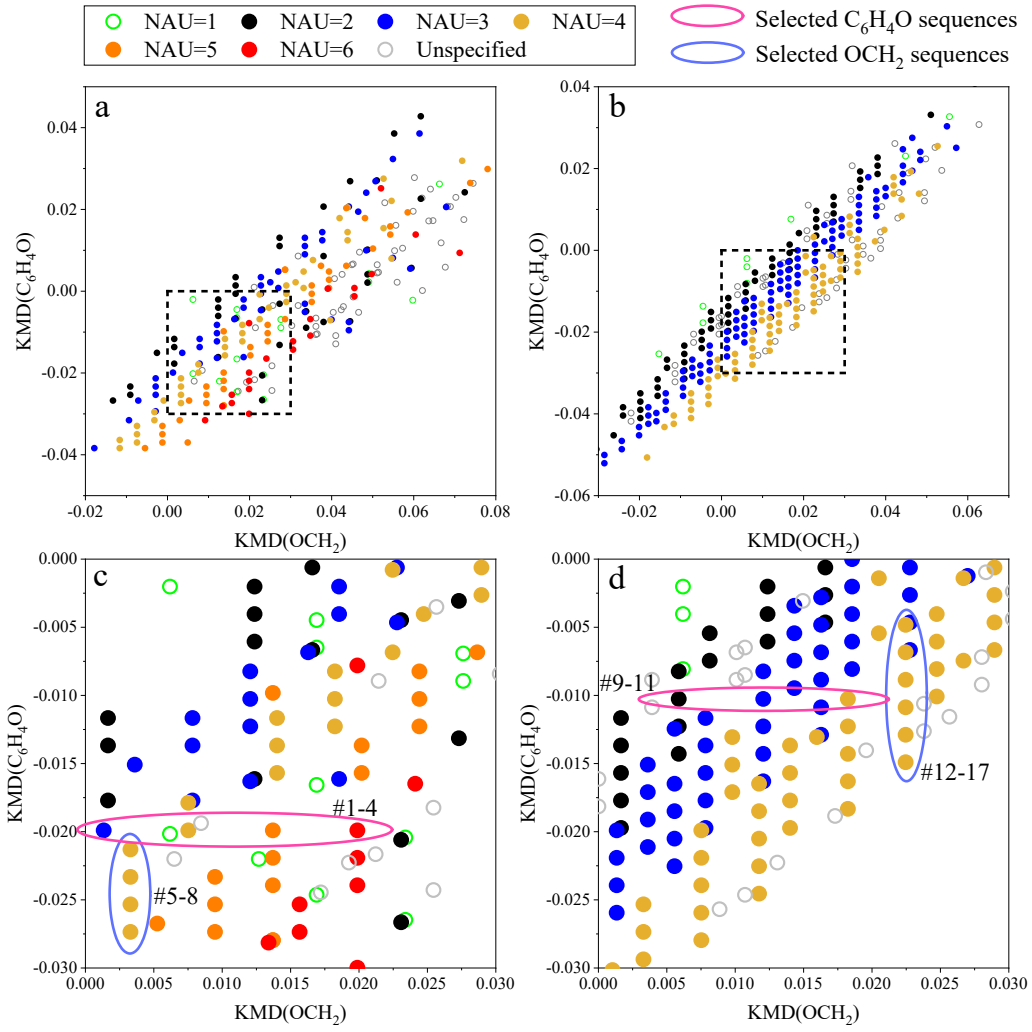

Fig. 8. C_6H_4O vs OCH_2 2D KMD plots for H- and G-derived heavy components, with colors indicating different number of aromatic units. a) Full range of H-derived oligomers; b) full range of G-derived oligomers; c) zoomed-in region of H-derived oligomers; d; zoomed-in region of G-derived oligomers.

through the condensation of aromatic oligomers.

On average, gaining of one aromatic ring happens along with the addition of 7–8 carbon atoms and 4 DBE approximately for both H- and G-derived oligomers (Table 5). As a benzene ring already corresponds to 6 carbon atoms and 4 DBE, this means the newly-attached aromatic rings typically have very simple side-chain structures and almost no additional unsaturated bonds.

3.3. *Evolution of heavy components through specific reaction pathways*

As verified above (Table 5), the newly attached aromatic rings during the re-polymerization have very simple side-chain structures. Phenol is one of the simplest modified monomers in H- and G-pyrolysis liquid products (Table 3), which is likely to be the most important aromatic units that link together during re-polymerization. This has been verified by using other aromatic building blocks as y-axis KMD base with inadequate visualization effects on 2D KMD plots. Therefore, the phenol core (C_6H_4O) was chosen as the fixed y-axis KMD base, to represent the evolution of various aromatic units [12]. Based on the possible modifications of basic functional groups [26], OCH_2, CO, CH_2, CO_2, O and H_2O were successively chosen as the x-axis KMD base, thus creating 6 different 2D KMD plots for both H- and G-derived heavy components (Fig. S2, S3). Significantly more series of vertical variations can be seen from the KMD(C_6H_4O) vs KMD(OCH_2) plots, indicating oligomers' evolution via methoxylation reactions as a major pathway (Fig. S2a, S3a). Therefore, the KMD(C_6H_4O) vs KMD(OCH_2) plots are reprinted with zoomed-in figures for better comparison (Fig. 8). Although it is mathematically possible that the results of other modifications combined together lead to the same modification in molecular formulas, it is highly improbable that such modifications always happen in exactly the same quantity for each component so as to form the OCH_2 or C_6H_4O sequences with such regular distribution pattern.

Both H- and G-derived oligomers distribute to the 2D KMD in a quite regular manner, as most of the components can be found in either horizontal sequences (phenol core addition) or vertical sequences (methoxylation). Horizontally, up to 5 phenol cores can be attached to H-derived monomers to form oligomers with various NAU; while in most cases, only 2 phenol cores at most can be attached to G-derived monomers. This is because less phenol was actually generated in the G-derived monomers than in the H-derived monomers (Table 3), which is the dominant building blocks to form oligomers with higher NAU (Fig. 7). On the contrary, less methoxy groups (only 2 or 3) can be attached to H-derived benzene rings through vertical variations; while the G-derived methoxy sequences mostly contain 4–6 oligomeric variations. Therefore, it is speculated that these two functional groups are in competition for the linking positions on the benzene rings. The detailed statistical

Table 6
Detailed statistical information of detected sequences in Fig. 8.

	OCH_2 sequences in H	OCH_2 sequences in G	C_6H_4O sequences in H	C_6H_4O sequences in G
Number of sequences	61	86	55	95
Average number of components in each sequence	2.72	3.17	2.64	2.53

Table 7
Chemical formulas of circled oligomers in Fig. 8, as examples of evolution sequences in 2D KMD plots.

Selected sequences	No.	Formula	KMD(C_6H_4O)	KMD(OCH_2)
C_6H_4O sequence in H	1	$C_{21}H_{16}O_3$	−0.0199	0.0013
	2	$C_{27}H_{20}O_4$	−0.0199	0.0075
	3	$C_{33}H_{24}O_5$	−0.0199	0.0137
	4	$C_{39}H_{28}O_6$	−0.0199	0.0199
OCH_2 sequence in H	5	$C_{25}H_{18}O_3$	−0.0213	0.0033
	6	$C_{26}H_{20}O_4$	−0.0233	0.0033
	7	$C_{27}H_{22}O_5$	−0.0253	0.0033
	8	$C_{28}H_{24}O_6$	−0.0273	0.0033
C_6H_4O sequence in G	9	$C_{15}H_{12}O_3$	−0.0103	0.0059
	10	$C_{21}H_{16}O_3$	−0.0103	0.0121
	11	$C_{27}H_{20}O_4$	−0.0103	0.0182
OCH_2 sequence in G	12	$C_{27}H_{18}O_4$	−0.0048	0.0225
	13	$C_{28}H_{20}O_5$	−0.0068	0.0225
	14	$C_{29}H_{22}O_6$	−0.0089	0.0225
	15	$C_{30}H_{24}O_7$	−0.0109	0.0225
	16	$C_{31}H_{26}O_8$	−0.0129	0.0225
	17	$C_{32}H_{28}O_9$	−0.0149	

information is provided in Table 6, including number of sequences and average number of components in each sequence. One example is selected for each kind of sequences (circled out in Fig. 8a, 5b), with their chemical formulas listed in Table 7. In the H-selected C_6H_4O sequence for example, the addition of every C_6H_4O in formula causes the KMD (OCH_2) to increase for a same value of 0.0062, while the KMD(C_6H_4O) remains the same. This explains the utility of 2D KMD plots for quickly identifying structurally related compounds. To reveal the influence of temperature on the distribution of oligomers within OCH_2 or C_6H_4O sequences, they are compared in terms of relative peak abundance (Fig. 9). For the first appearing formula in each sequence, the adding group number (*x*-axis) is set as zero. Both reaction pathways (methoxylation and phenol core modification) are favored in G-derived oligomers, as indicated in the magnitude of abundance. For both samples, the adding number of phenol cores is mostly restricted to 2, while more methoxy groups can be added. The rising temperature inhibits the evolution of G-derived oligomers via the two reaction pathways, as their abundance within both sequences reduces sharply. In case of H-derived oligomers, higher temperature only inhibits the adding of OCH_2 to <2 groups.

3.4. *Speculation of structural information through 2D KMD evolution*

The implementation of 2D KMD plots is helpful for identifying series of homologous compounds (Fig. 8). This kind of information enables exhibiting groups of components that link together through the variations of specific functional groups [26]. In specific cases in which there is existing structural information about one or some of the identified formulas in a group, it is possible to speculate the structures of other formulas in the same group. A proof-of-concept demonstration of this strategy is illustrated in Fig. 10. Model compound H ($C_7H_6O_2$) is

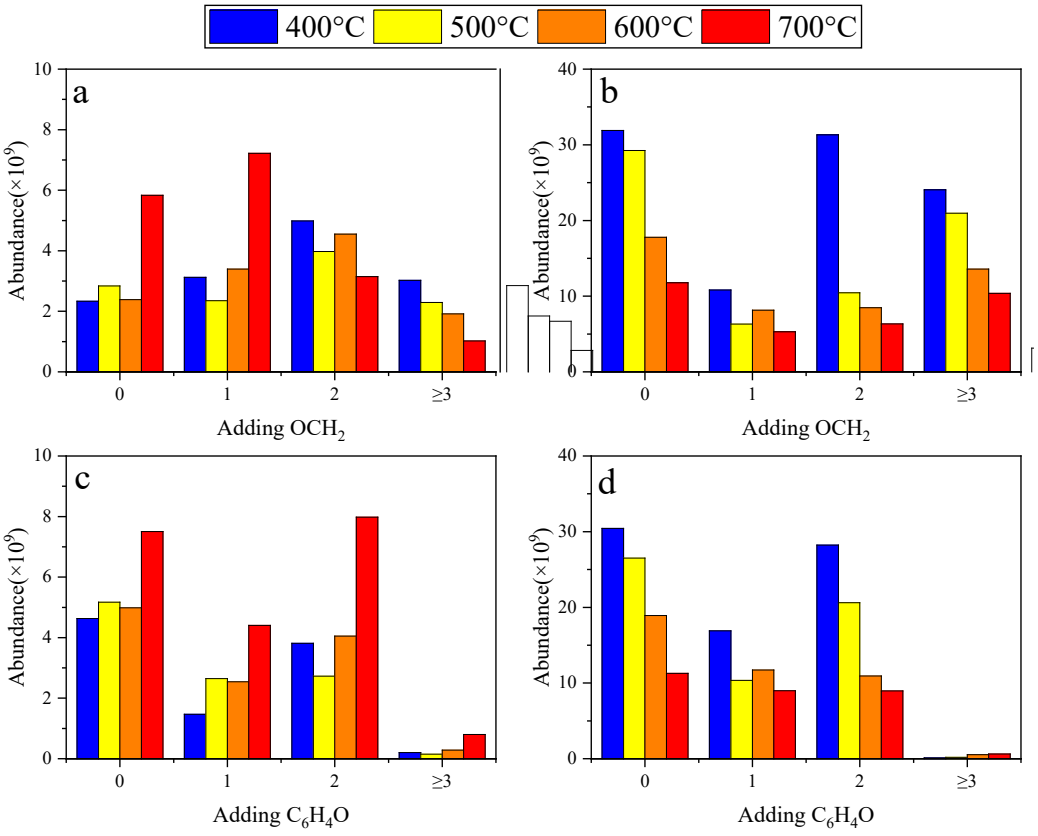

Fig. 9. Abundance distribution of oligomers within OCH_2 or C_6H_4O sequences for different temperatures. a) H-derived oligomers in OCH_2 sequences; b) G-derived oligomers in OCH_2 sequences; c) H-derived oligomers in C_6H_4O sequences; d) G-derived oligomers in C_6H_4O sequences.

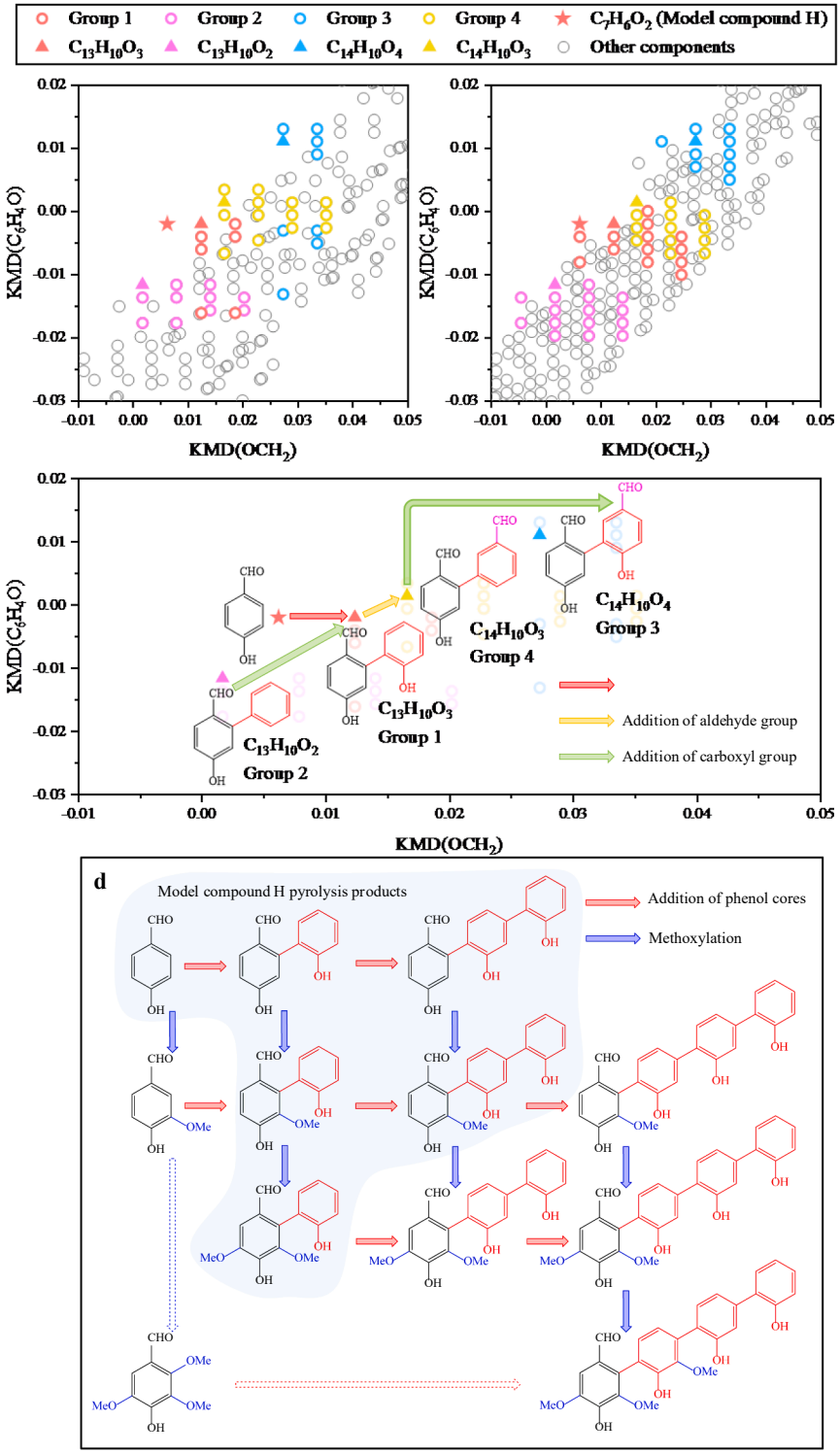

Fig. 10. Pathways of methoxy or phenol core modifications inside different groups of a) H-derived heavy components and b) G-derived heavy components. c) Proposed correlations of structure between triangular dimers in each group. d) Bottom Proposed structures and reaction pathways of heavy components in Group 1, starting from $C_7H_6O_2$, with H-derived components in dashed box). Note that the linking positions of functional groups are illustrative.

proposed to be a starting compound with identified structural information (4-hydroxybenzaldehyde). The 2D KMD plots certifies that molecules inside a specific group (group 1 for example, Fig. 9d) evolve through the modifications of methoxy (vertically) or phenol cores (horizontally). Therefore, by attaching a phenol core to the benzene ring, 4-hydroxybenzaldehyde can form $C_{13}H_{10}O_3$, which then correlates to the triangular molecules in other groups through the modification of hydroxyl or aldehyde groups (Fig. 9c). These reactions are speculated because similar behaviors prevail in the side chain conversion among light liquid products. Additionally, these triangular molecules can also act as a starting molecule inside their own groups and create similar evolving routes like those illustrated in Fig. 10d.

This approach can be expanded to other functional groups as well since the modification of functional groups other than OCH_2 or C_6H_4O will cause a regular movement with fixed length and slope on 2D KMD plots [40]. In this sense, the number of reaction pathways that can be simultaneously visualized in single 2D KMD plot are expanded to more than two. Therefore, this approach enables speculating structural information of much more molecule formulas derived from FT-ICR-MS with limited already-identified molecules. Moreover, this approach may also be feasible for macromolecules other than lignin.

4. Conclusions

The pyrolysis heavy components from two lignin model compounds were analyzed and identified at molecular scale using FT-ICR-MS. The detected heavy components are mostly phenolic oligomers distributed in the nominal mass range of 200–600 Da with 2–6 aromatic rings, each possessing 7–8 carbon atoms and 4 DBE on average. However, more non-phenolic structures (such as lipids and unsaturated hydrocarbons) are detected in lignin-oil heavy components, indicating that aromatic structures are better preserved during the pyrolysis of these model compounds than of lignin, which is a preferred feature for deriving useful chemicals. These phenolic oligomers are assumed to be formed through the re-polymerization of certain GC-MS-detected monomers during pyrolysis. In particular, the extra methoxy group in model compound G allows for more side-chain conversion reactions, creating more variations of monomer products as building blocks for heavy components and char. With the visualization on 2D KMD plots, two evolution pathways of heavy components were found to be dominant, namely the modification of phenol cores and methoxy groups, which are favored by H-derived heavy components and G-derived heavy components, respectively. Aldehyde groups promote the evolution of heavy components with more aromatic rings (up to 6), which might serve as char precursors. Such influence is mitigated by the co-existence of methoxy groups, which might compete for the linking positions on benzene rings. This also explains the higher char yield during pyrolysis of monomer H (aldehyde group) than that of monomer G (aldehyde group and methoxy group). The rising temperature generally inhibits the evolution of oligomers through the two pathways, which also explain the lower char yields at higher temperatures.

CRediT authorship contribution statement

Yi Qiu: Writing – original draft, Software, Visualization. **Dian Zhong:** Writing – review & editing, Methodology, Formal analysis. **Kuo Zeng:** Writing – review & editing, Methodology, Formal analysis. **Jun Li:** Investigation, Software. **Gilles Flamant:** Methodology, Formal analysis. **Ange Nzihou:** Investigation, Formal analysis, Visualization. **Haiping Yang:** Conceptualization, Resources, Validation. **Hanping Chen:** Validation.

Declaration of Competing Interest

The authors declare that they have no known competing financial interests or personal relationships that could have appeared to influence the work reported in this paper.

Data availability

No data was used for the research described in the article.

Acknowledgements

Authors acknowledge funding from the National Key R&D Program of China (2017YFE0124200), the National Natural Science Foundation of China (52076098) and The Young Top-notch Talent Cultivation Program of Hubei Province. The FT-ICR-MS test was provided by Analytical & Testing Center of Huazhong University of Science & Technology. There are no conflicts to declare.

Appendix A. Supplementary data

Supplementary data to this article can be found online at https://doi.org/10.1016/j.fuel.2022.125333.

References

[1] Schutyser W, Renders T, Van den Bosch S, Koelewijn SF, Beckham GT, Sels BF. Chemicals from lignin: an interplay of lignocellulose fractionation, depolymerisation, and upgrading. Chem Soc Rev 2018;47(3):852–908.
[2] Sun Z, Fridrich B, de Santi A, Elangovan S, Barta K. Bright Side of Lignin Depolymerization: Toward New Platform Chemicals. Chem Rev 2018;118(2):614–78.
[3] Wang L, Li J, Chen Y, Yang H, Shao J, Zhang X, et al. Investigation of the pyrolysis characteristics of guaiacol lignin using combined Py-GC x GC/TOF-MS and in-situ FTIR. Fuel 2019;251:496–505.
[4] Ralph J, Lapierre C, Boerjan W. Lignin structure and its engineering. Curr Opin Biotechnol 2019;56:240–9.
[5] Zakzeski J, Bruijnincx PCA, Jongerius AL, Weckhuysen BM. The Catalytic Valorization of Lignin for the Production of Renewable Chemicals. Chem Rev 2010;110(6):3552–99.
[6] Garcia Calvo-Flores F, Dobado JA. Lignin as Renewable Raw Material. ChemSusChem 2010;3(11):1227–35.
[7] Friar E. Plant Cells and Their Organelles. Crop Sci 2017;57(6):3360–1.
[8] Chua YW, Yu Y, Wu H. Thermal decomposition of pyrolytic lignin under inert conditions at low temperatures. Fuel 2017;200:70–5.
[9] Esposito D, Antonietti M. Redefining biorefinery: the search for unconventional building blocks for materials. Chem Soc Rev 2015;44(16):5821–35.
[10] Cao Y, Chen SS, Zhang S, Ok YS, Matsagar BM, Wu KCW, et al. Advances in lignin valorization towards bio-based chemicals and fuels: Lignin biorefinery. Bioresour Technol 2019;291.
[11] M.A. Atmodjo, Z. Hao, D. Mohnen, Evolving Views of Pectin Biosynthesis, in: S.S. Merchant (Ed.), Annual Review of Plant Biology, Vol 642013, pp. 747-+.
[12] Qi Y, Hempelmann R, Volmer DA. Two-dimensional mass defect matrix plots for mapping genealogical links in mixtures of lignin depolymerisation products. Anal Bioanal Chem 2016;408(18):4835–43.
[13] Liu C, Deng Y, Wu S, Mou H, Liang J, Lei M. Study on the pyrolysis mechanism of three guaiacyl-type lignin monomeric model compounds. J Anal App Pyrolysis 2016;118:123–9.
[14] Jiang G, Nowakowski DJ, Bridgwater AV. Effect of the Temperature on the Composition of Lignin Pyrolysis Products. Energy Fuels 2010;24(8):4470–5.
[15] Galkin MV, Samec JSM. Lignin Valorization through Catalytic Lignocellulose Fractionation: A Fundamental Platform for the Future Biorefinery. ChemSusChem 2016;9(13):1544–58.
[16] Hosoya T, Kawamoto H, Saka S. Role of methoxyl group in char formation from lignin-related compounds. J Anal Appl Pyrol 2009;84(1):79–83.
[17] Wang H, Pu Y, Ragauskas A, Yang B. From lignin to valuable products-strategies, challenges, and prospects. Bioresour Technol 2019;271:449–61.
[18] Asmadi M, Kawamoto H, Saka S. Thermal reactions of guaiacol and syringol as lignin model aromatic nuclei. J Anal Appl Pyrol 2011;92(1):88–98.
[19] Jiang W, Chu J, Wu S, Lucia LA. Modeling the pyrolytic behavior of lignin through two representative monomers: Vanillin and acetovanillone. J Anal Appl Pyrol 2018;130:241–8.
[20] Bai X, Kim KH, Brown RC, Dalluge E, Hutchinson C, Lee YJ, et al. Formation of phenolic oligomers during fast pyrolysis of lignin. Fuel 2014;128:170–9.
[21] Long J, Xu Y, Wang T, Yuan Z, Shu R, Zhang Q, et al. Efficient base-catalyzed decomposition and in situ hydrogenolysis process for lignin depolymerization and char elimination. Appl Energy 2015;141:70–9.
[22] Kozliak EI, Kubatova A, Artemyeva AA, Nagel E, Zhang C, Rajappagowda RB, et al. Thermal Liquefaction of Lignin to Aromatics: Efficiency, Selectivity, and Product Analysis. ACS Sustain Chem Eng 2016;4(10):5106–22.
[23] Andrianova AA, DiProspero T, Geib C, Smoliakova IP, Kozliak EI, Kubatova A. Electrospray Ionization with High-Resolution Mass Spectrometry as a Tool for Lignomics: Lignin Mass Spectrum Deconvolution. J Am Soc Mass Spectrom 2018;29(5):1044–59.
[24] Zhang X, Chen L, Kong W, Wang T, Zhang Q, Long J, et al. Upgrading of bio-oil to boiler fuel by catalytic hydrotreatment and esterification in an efficient process. Energy 2015;84:83–90.
[25] Michailof CM, Kalogiannis KG, Sfetsas T, Patiaka DT, Lappas AA. Advanced analytical techniques for bio-oil characterization. Wiley Interdiscip Rev-Energy Environ 2016;5(6):614–39.
[26] Terrell E, Carre V, Dufour A, Aubriet F, Le Brech Y, Garcia-Perez M. Contributions to Lignomics: Stochastic Generation of Oligomeric Lignin Structures for Interpretation of MALDI-FT-ICR-MS Results. ChemSusChem 2020;13(17):4428–45.
[27] Zhang R, Qi Y, Ma C, Ge J, Hu Q, Yue F-J, et al. Characterization of Lignin Compounds at the Molecular Level: Mass Spectrometry Analysis and Raw Data Processing. Molecules 2021;26(1).
[28] Cho Y, Ahmed A, Islam A, Kim S. Developments in FT-ICR MS instrumentation, ionization techniques, and data interpretation methods for petroleomics. Mass Spectrom Rev 2015;34(2):248–63.

[29] Bojkovic A, Vermeire FH, Kuzmanovic M, Thi HD, Van Geem KM. Analytics Driving Kinetics: Advanced Mass Spectrometric Characterization of Petroleum Products. Energy Fuels 2021.
[30] Shi Q, Zhang Y, Chung KH, Zhao S, Xu C. Molecular Characterization of Fossil and Alternative Fuels Using Electrospray Ionization Fourier Transform Ion Cyclotron Resonance Mass Spectrometry: Recent Advances and Perspectives. Energy Fuels 2021;35(22):18019–55.
[31] Zark M, Dittmar T. Universal molecular structures in natural dissolved organic matter. Nat Commun 2018;9.
[32] Gong C, Jiao R, Yan W, Yu Q, Li Q, Zhang P, et al. Enhanced chemodiversity, distinctive molecular signature and diurnal dynamics of dissolved organic matter in streams of two headwater catchments, Southeastern China. Water Res 2022;211.
[33] Zhang X, Han J, Zhang X, Shen J, Chen Z, Chu W, et al. Application of Fourier transform ion cyclotron resonance mass spectrometry to characterize natural organic matter. Chemosphere 2020;260.
[34] Letourneau DR, Volmer DA. Mass spectrometry-based methods for the advanced characterization and structural analysis of lignin: A review. Mass Spectrom Rev 2021.
[35] Lozano DCP, Jones HE, Reina TR, Volpe R, Barrow MP. Unlocking the potential of biofuels via reaction pathways in van Krevelen diagrams. Green Chem 2021;23 (22):8949–63.
[36] Terrell E, Garcia-Perez M. Novel Strategy To Analyze Fourier Transform Ion Cyclotron Resonance Mass Spectrometry Data of Biomass Pyrolysis Oil for Oligomeric Structure Assignment. Energy Fuels 2020;34(7):8466–81.
[37] Li J, Xiong Z, Zeng K, Zhong D, Zhang X, Chen W, et al. Characteristics and Evolution of Nitrogen in the Heavy Components of Algae Pyrolysis Bio-Oil. Environ Sci Technol 2021;55(9):6373–85.
[38] Zhong D, Zeng K, Li J, Qiu Y, Flamant G, Nzihou A, et al. Characteristics and evolution of heavy components in bio-oil from the pyrolysis of cellulose, hemicellulose and lignin. Renew Sustain Energy Rev 2022;157:111989.
[39] Hertzog J, Mase C, Hubert-Roux M, Afonso C, Giusti P, Barrere-Mangote C. Characterization of Heavy Products from Lignocellulosic Biomass Pyrolysis by Chromatography and Fourier Transform Mass Spectrometry: A Review. Energy Fuels 2021;35(22):17979–8007.
[40] Kim S, Kramer RW, Hatcher PG. Graphical method for analysis of ultrahigh-resolution broadband mass spectra of natural organic matter, the van Krevelen diagram. Anal Chem 2003;75(20):5336–44.
[41] Hughey CA, Hendrickson CL, Rodgers RP, Marshall AG, Qian KN. Kendrick mass defect spectrum: A compact visual analysis for ultrahigh-resolution broadband mass spectra. Anal Chem 2001;73(19):4676–81.
[42] Bae E, Na J-G, Chung SH, Kim HS, Kim S. Identification of about 30 000 Chemical Components in Shale Oils by Electrospray Ionization (ESI) and Atmospheric Pressure Photoionization (APPI) Coupled with 15 T Fourier Transform Ion Cyclotron Resonance Mass Spectrometry (FT-ICR MS) and a Comparison to Conventional Oil. Energy Fuels 2010;24(4):2563–9.
[43] Dhungana B, Becker C, Zekavat B, Solouki T, Hockaday WC, Chambliss CK. Characterization of Slow-Pyrolysis Bio-Oils by High-Resolution Mass Spectrometry and Ion Mobility Spectrometry. Energy Fuels 2015;29(2):744–53.
[44] Qiu Y, Zhong D, Zeng K, Li J, Flamant G, Nzihou A, et al. Effects of cellulose-lignin interaction on the evolution of biomass pyrolysis bio-oil heavy components. Fuel 2022;323:124413.
[45] Xiong Z, Han H, Azis MM, Hu X, Wang Y, Su S, et al. Formation of the heavy tar during bio-oil pyrolysis: A study based on Fourier transform ion cyclotron resonance mass spectrometry. Fuel 2019;239:108–16.
[46] Hu S, Han H, Syed-Hassan SSA, Zhang Y, Wang Y, Zhang L, et al. Evolution of heavy components during sewage sludge pyrolysis: A study using an electrospray ionization Fourier transform ion cyclotron resonance mass spectrometry. Fuel Process Technol 2018;175:97–103.
[47] Cole DP, Smith EA, Dalluge D, Wilson DM, Heaton EA, Brown RC, et al. Molecular characterization of nitrogen-containing species in switchgrass bio-oils at various harvest times. Fuel 2013;111:718–26.
[48] Miettinen I, Makinen M, Vilppo T, Janis J. Compositional Characterization of Phase-Separated Pine Wood Slow Pyrolysis Oil by Negative-Ion Electrospray Ionization Fourier Transform Ion Cyclotron Resonance Mass Spectrometry. Energy Fuels 2015;29(3):1758–65.
[49] Stas M, Chudoba J, Auersvald M, Kubicka D, Conrad S, Schulzke T, et al. Application of orbitrap mass spectrometry for analysis of model bio-oil compounds and fast pyrolysis bio-oils from different biomass sources. J Anal Appl Pyrol 2017; 124:230–8.
[50] Wang J, Hao Z, Shi F, Yin Y, Cao D, Yao Z, et al. Characterization of Brominated Disinfection Byproducts Formed During the Chlorination of Aquaculture Seawater. Environ Sci Technol 2018;52(10):5662–70.
[51] Koch BP, Dittmar T, Witt M, Kattner G. Fundamentals of molecular formula assignment to ultrahigh resolution mass data of natural organic matter. Anal Chem 2007;79(4):1758–63.
[52] Ohno T, Ohno PE. Influence of heteroatom pre-selection on the molecular formula assignment of soil organic matter components determined by ultrahigh resolution mass spectrometry. Anal Bioanal Chem 2013;405(10):3299–306.
[53] Koch BP, Witt MR, Engbrodt R, Dittmar T, Kattner G. Molecular formulae of marine and terrigenous dissolved organic matter detected by electrospray ionization Fourier transform ion cyclotron resonance mass spectrometry. Geochim Cosmochim Acta 2005;69(13):3299–308.
[54] Hosoya T, Kawamoto H, Saka S. Pyrolysis gasification reactivities of primary tar and char fractions from cellulose and lignin as studied with a closed ampoule reactor. J Anal Appl Pyrol 2008;83(1):71–7.
[55] Zhu G, Ouyang X, Jiang L, Zhu Y, Jin D, Pang Y, et al. Effect of functional groups on hydrogenolysis of lignin model compounds. Fuel Process Technol 2016;154:132–8.
[56] Furutani Y, Dohara Y, Kudo S, Hayashi J, Norinaga K. Theoretical Study on the Kinetics of Thermal Decomposition of Guaiacol and Catechol. J Phys Chem A 2017; 121(44):8495–503.